Synergistically Engineered NiCoMn-LDH@Carbon Nanofibers for Boosted Electrochemical Charge Storage and High-Energy Supercapacitors

Saranraj A[1,3,4], M. N. M. Ansari [2], Varghese Samuel [5], Mani Govindasamy [3,4*], Sujin P Jose [1**]

[1] Advanced Materials Laboratory, School of Physics, Madurai Kamaraj University, Madurai- 625021, Tamil Nadu, India

[2] Institute of Power Engineering, Universiti Tenaga Nasional, 43000, Kajang, Selangor, Malaysia

[3] International Ph.D. Program in Innovative Technology of Biomedical Engineering and Medical Devices, Ming Chi University of Technology, New Taipei City 243303, Taiwan

[4]Research Center for Intelligence Medical Devices, Ming Chi University of Technology, New Taipei City 243303, Taiwan.

[5]Matlab Technologies, Thane 421302, Maharashtra, India

[*] Corresponding author: Email: sujamystica@yahoo.com, govindasamy420700@gmail.com

Supporting Information

Calculation formula:

The gravimetric specific capacitance (C, F g^{-1}) and charge (Q, mAh g^{-1}) were calculated by following equation (1) and (2)

$$C = \frac{I \times \Delta t}{m \times \Delta V} \quad (1)$$

$$Q = \frac{I \times \Delta t}{3.6 \times m} \quad (2)$$

where I (A), Δt (s), m (g), and ΔV (V) represent current density, discharge time, the weight of active materials, and the potential window, respectively.

The power density P (W kg^{-1}) and energy density E (Wh kg^{-1}) of the SSC were calculated via following equations (5) and (6):

$$E = \frac{Q \times V}{M} \quad (3)$$

$$P = \frac{E}{\Delta t} \quad (4)$$

where Q (C), V (V), M (g), and Δt (s) represent the quantity of electric charge, the average voltage of symmetric supercapacitor, the total weight of positive and negative electrode materials, and the discharge time respectively.

Evaluation of Specific Capacitance and Charge Storage Capacity

In this study, we evaluated the charge storage performance of a pseudocapacitive material by determining its specific capacitance and the corresponding charge storage capacity. The material was tested under galvanostatic conditions at a current density of 1 A/g within a voltage window of 0.45 V.

Calculation of Specific Capacitance

The specific capacitance (C_{sp}) is determined using the galvanostatic discharge method and the following equation:

$C_{sp} = (I \times \Delta t) / (m \times \Delta V)$

where:

I is the discharge current (A), Δt is the discharge time (s), m is the mass of the active electrode material (g), ΔV is the voltage window (V).

Using this method, the measured specific capacitance for the electrode material was determined to be:

C_{sp} = 1783 Fg^{-1} at 1 Ag^{-1}

Calculation of Charge Storage Capacity

The total charge stored per gram (specific capacity) is calculated from the capacitance using the relationship:

$Q_{sp} = C_{sp} \times \Delta V$

Substituting the known values:

$Q_{sp} = 1783\ Fg^{-1} \times 0.45\ V \approx \mathbf{802.35\ C\ g^{-1}}$

To express this capacity in terms of milliampere-hours per gram (mAh/g), we use the conversion factor:

1 mAh = 3.6 C

Thus, the specific capacity in mAh/g is given by:

$Q_{sp}\ (mAh\ g^{-1}) = 802.35\ C\ g^{-1} \div 3.6 \approx \mathbf{222.88\ mAh\ g^{-1}}$

Discussion

For an ideal capacitor, the stored charge Q is linearly related to the applied voltage by the equation:

$Q = C \times V$

This implies that the specific capacity would scale linearly with the voltage if the capacitance remains constant. In our evaluation, despite the pseudocapacitive nature of the material (where the capacitance may vary with voltage due to redox reactions), the narrow voltage window of 0.45 V permits the use of the linear approximation. This standard approach provides a straightforward means of comparison with other materials reported in the literature.

The high specific capacitance value of 1783 Fg^{-1} indicates that the electrode material has an exceptional ability to store charge per unit mass. When combined with the voltage window, this yields a specific capacity of approximately 802.35 C g^{-1} (or 222.88 mAh g^{-1}).

Electrochemical Studies of Individual samples

Three electrode system

NCM-LDH alone

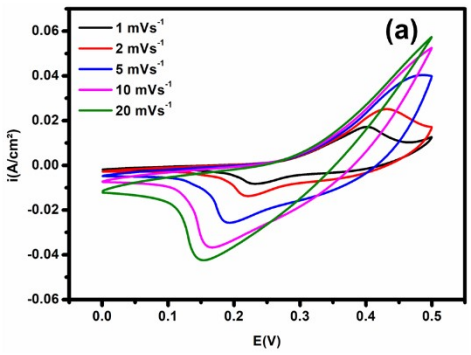

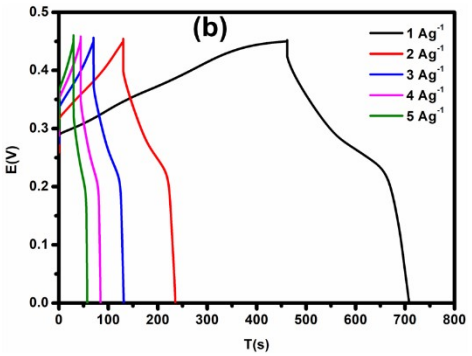

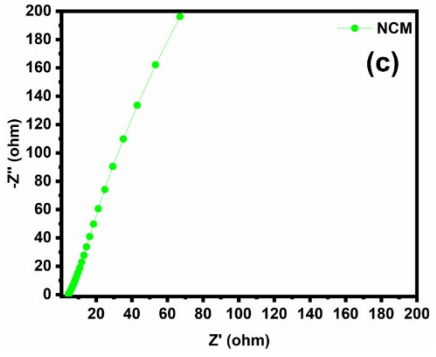

CNF alone

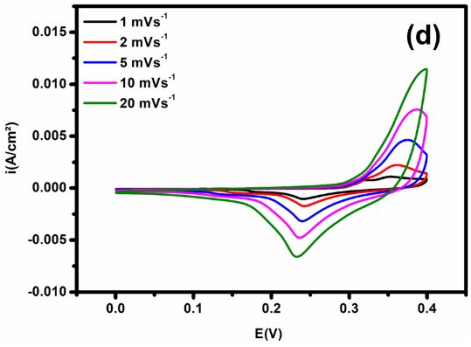

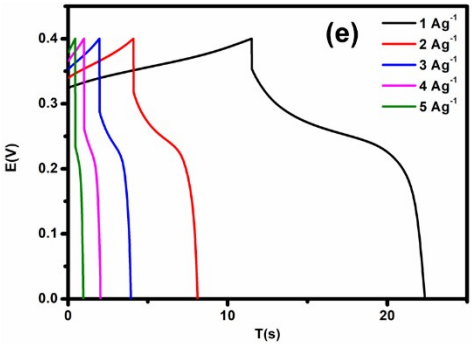

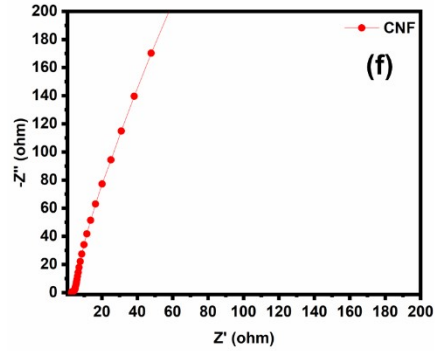

NCM-LDH@CNF (1:1)

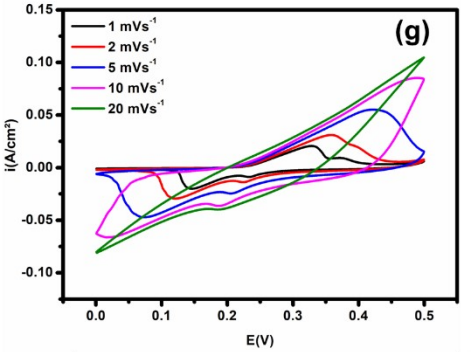

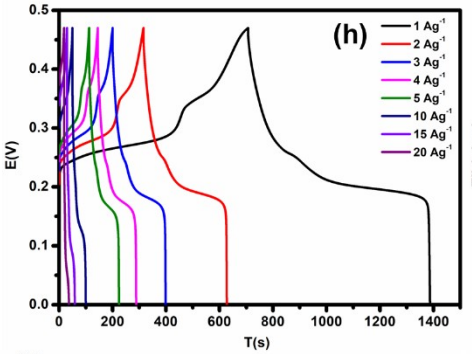

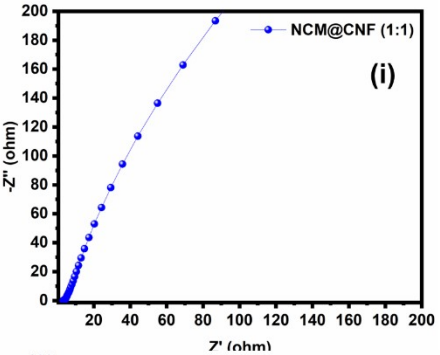

NCM-LDH@CNF (1:2)

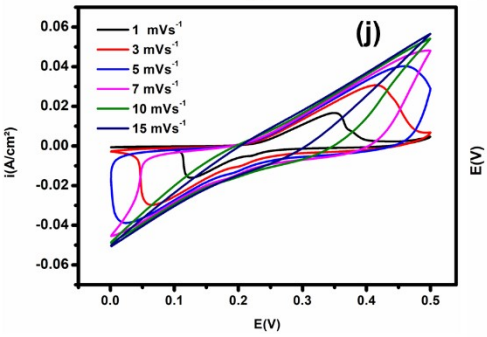

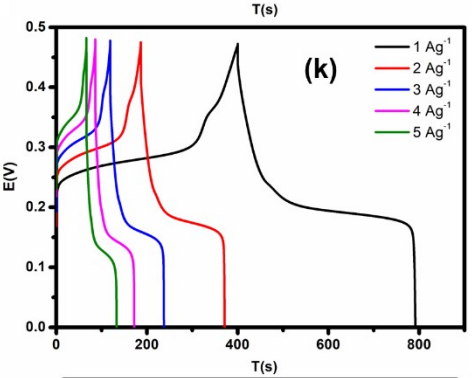

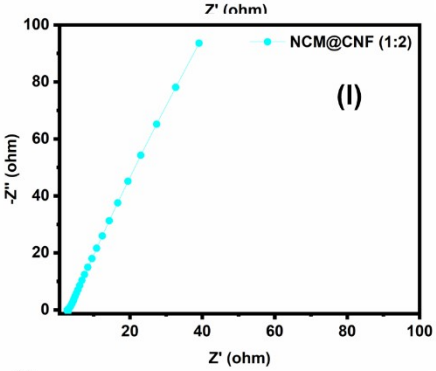

NCM-LDH@CNF (2:1)

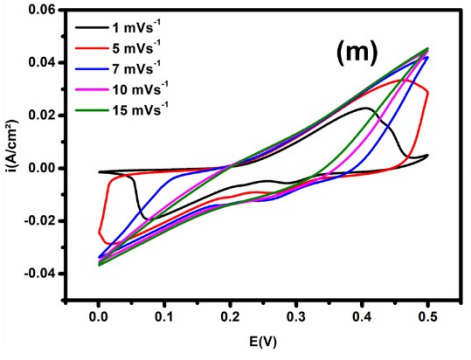

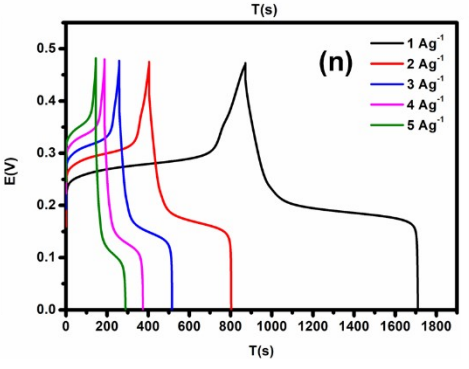

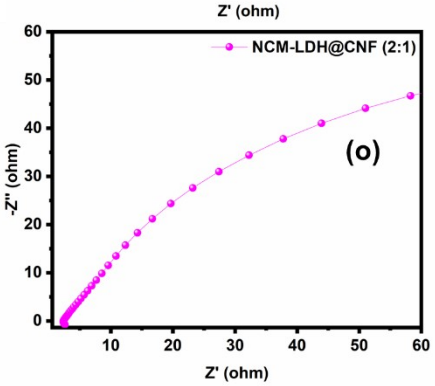

Fig. S1 Electrochemical characterization of different electrode materials. (a, d, g, j, m) Cyclic voltammetry (CV) curves at different scan rates, showing charge storage behaviour. (b, e, h, k, n) Galvanostatic charge-discharge (GCD) curves at various current densities, illustrating capacitance and charge retention. (c, f, i, l, o) Electrochemical impedance spectroscopy (EIS) Nyquist plots, depicting charge transfer resistance and conductivity. The comparison across different compositions highlights the impact of material modifications on electrochemical performance.

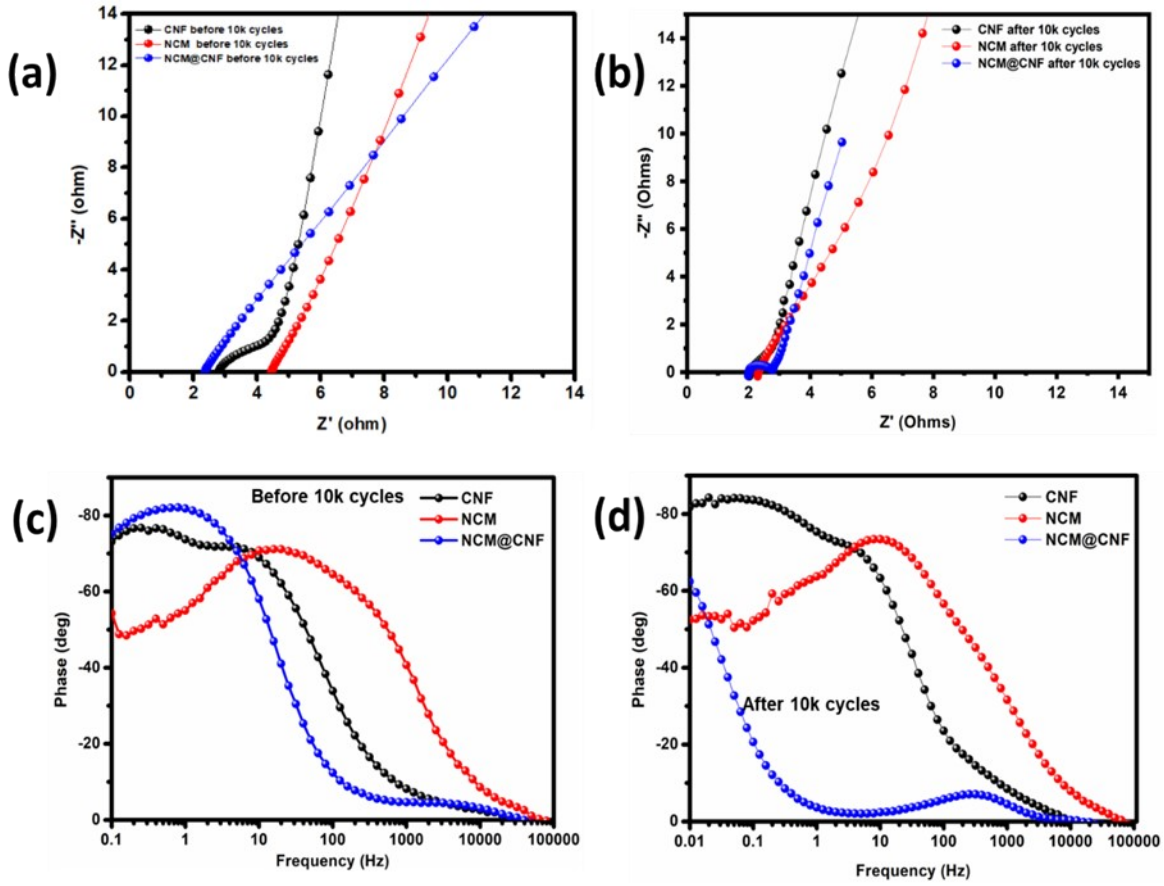

Fig. S2 Electrochemical impedance spectroscopy (EIS) and Bode phase plots of NiCoMn-LDH, CNF, and NiCoMn-LDH@CNF electrodes before and after 10,000 charge-discharge cycles.

(a) Nyquist plots before cycling, showing charge transfer resistance and diffusion behaviour.

(b) Nyquist plots after 10,000 cycles, illustrating improved conductivity and interface

stability, particularly for the NCM@CNF composite.

(c) Bode phase plots before cycling, indicating phase angles and frequency response characteristics.

(d) Bode phase plots after 10,000 cycles, showing retention of capacitive behaviour with a prominent shift in NCM@CNF, suggesting enhanced stability and ion diffusion properties.

Fig. S2 illustrates the electrochemical impedance spectroscopy (EIS) and Bode phase angle plots of NiCoMn-LDH, CNF, and NiCoMn-LDH@CNF electrodes before and after 10,000 charge-discharge cycles. Prior to cycling (Fig S2a), the NiCoMn-LDH@CNF electrode exhibits the lowest charge transfer resistance (R_{ct}) and a steep Warburg slope, indicating highly efficient ion diffusion and rapid charge transport. This enhanced behaviour can be attributed to the synergistic integration of the electroactive NiCoMn-LDH with the conductive CNF matrix. After 10,000 cycles (Fig S2b), a modest increase in R_{ct} is observed for NiCoMn-LDH@CNF, reflecting some structural or interfacial changes; however, it still outperforms both the individual CNF and NiCoMn-LDH electrodes, maintaining lower impedance and better electron/ion conductivity. The Bode phase plots (Fig S2c and S2d) show that NiCoMn-LDH@CNF initially achieves a phase angle close to −80°, indicative of excellent capacitive behaviour. Although the phase angle slightly decreases after long-term cycling, it retains significant capacitive features, confirming the robustness of the hybrid structure.

Statistical reproducibility of electrochemical performance

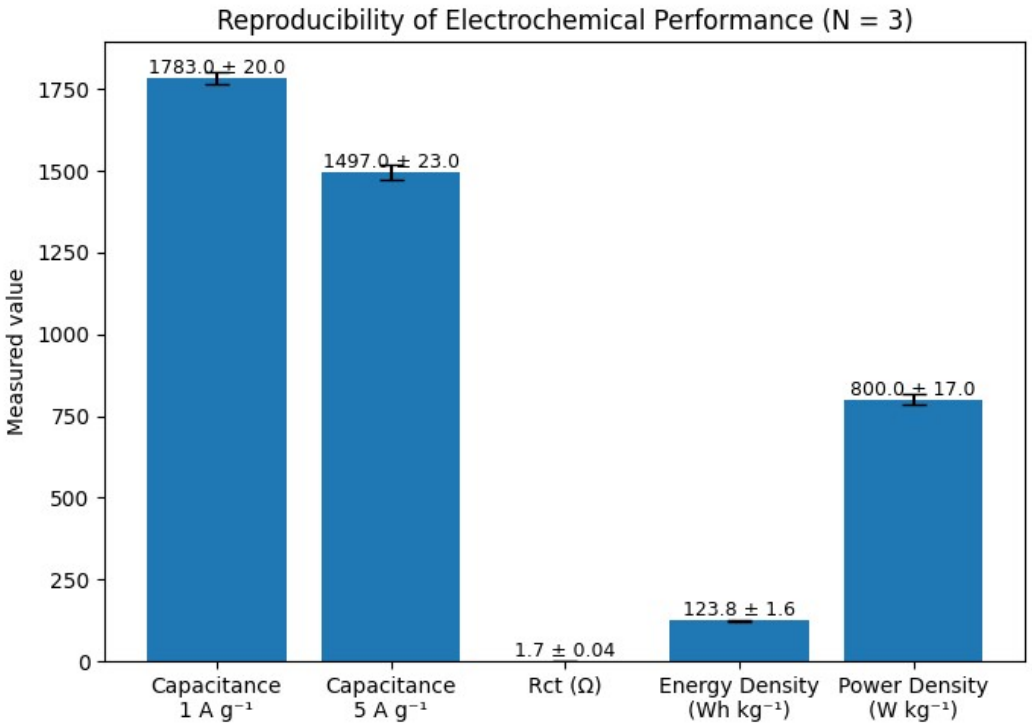

Fig. S3: Statistical reproducibility of electrochemical performance

Fig S3 illustrates the statistical reproducibility of the key electrochemical performance parameters of the assembled asymmetric supercapacitor (ASC) device. The specific capacitance measured at 1 A g^{-1} and 5 A g^{-1}, charge transfer resistance (Rct) obtained from electrochemical impedance spectroscopy, energy density, and power density were evaluated from three independent measurements (N = 3). The results are presented as mean values with error bars representing the standard deviation, and the numerical values (mean ± SD) are annotated directly on the bars. The small standard deviation across all parameters confirms the high reproducibility and reliability of the ASC device performance.

Table S1. Reproducibility analysis of electrochemical performance parameters

Parameter	**Replicate 1**	**Replicate 2**	**Replicate 3**	**Mean ± SD**
Specific capacitance at 1 A g^{-1} (F g^{-1})	1760	1795	1794	1783 ± 20
Specific capacitance at 5 A g^{-1} (F g^{-1})	1470	1505	1516	1497 ± 23
Charge transfer resistance, Rct (Ω)	1.65	1.72	1.73	1.70 ± 0.04
Energy density (Wh kg^{-1})	121.9	124.5	125.0	123.8 ± 1.6
Power density (W kg^{-1})	780	810	810	800 ± 17

The practical demonstration of the assembled device

Photographs of the assembled device Sequential images showing the device successfully powering LEDs over time, from (i) initial activation (0 min) to sustained operation (v) at 10.45 min.

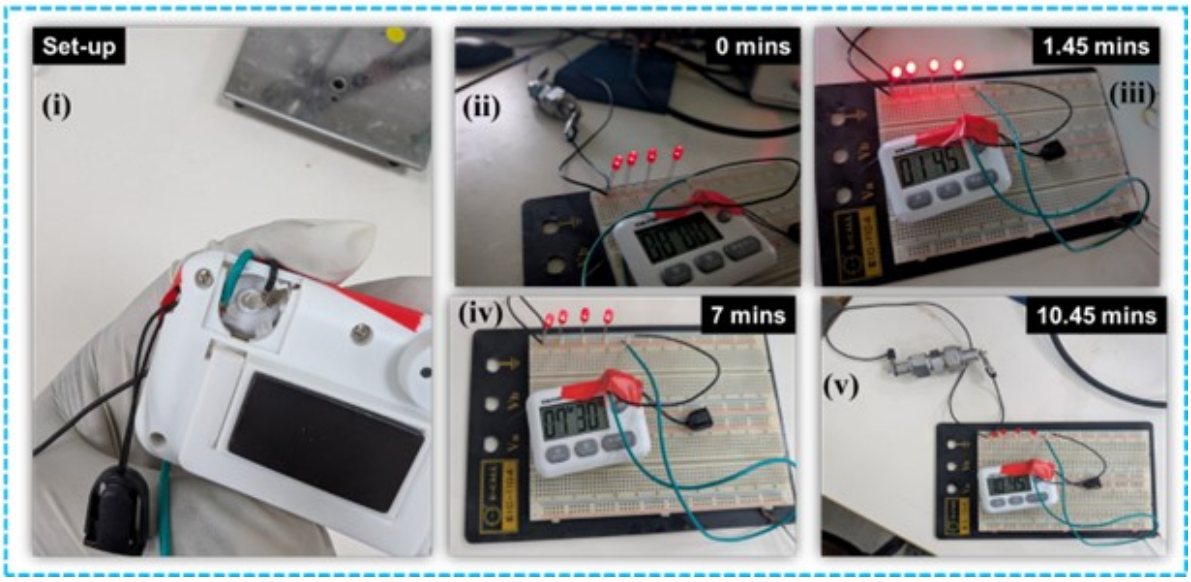

Fig. S4: The practical demonstration of the assembled device

Supplementary Notes for Charge Balance Calculation for Asymmetric Supercapacitor

The assembly of the asymmetric supercapacitor (ASC) device was carried out following the standard charge balance principle to ensure equal charge storage between the positive and negative electrodes ($q^+ = q^-$). The charge stored by each electrode is governed by the relation:

$$q = m \times C \times \Delta V$$

where m is the mass of active material (g), C is the specific capacitance (F g^{-1}), and ΔV is the potential window (V).

To achieve charge balance in the ASC device, the mass ratio between the positive and negative electrodes was determined using:

$$m^+ C^+ \Delta V^+ = m^- C^- \Delta V^-$$

or

$$\frac{m^+}{m^-} = \frac{C^- \Delta V^-}{C^+ \Delta V^+}$$

In the present study, the NiCoMn-LDH@CNF (2:1) electrode (positive electrode) exhibits a specific capacitance of ~1783 F g^{-1} at 1 A g^{-1} within a potential window of ~0-0.5 V. The activated carbon (AC) electrode (negative electrode) delivers a specific capacitance of ~307 F g^{-1} at 1 A g^{-1} within a potential window of ~–1.0-0 V.

Substituting these values:

$$\frac{m^+}{m^-} \approx \frac{307 \times 1.0}{1783 \times 0.5} \approx 0.34$$

Accordingly, the mass loading of the electrodes was adjusted to satisfy this ratio during device fabrication. [**5 mg (NiCoMn-LDH@CNF) // 15 mg (AC)]**

The effectiveness of this charge balancing is further confirmed by the nearly symmetric galvanostatic charge-discharge profiles, high coulombic efficiency (~100%), and stable cycling performance (≈80% capacitance retention after 10,000 cycles), indicating reliable and well-balanced device operation.

Table S2: Electrochemical performance metrics of the various materials evaluated at current densities ranging from 1 A g^{-1} to 5 A g^{-1} under both two-electrode and three-electrode configurations.

Current density (A g^{-1})	Specific capacitance of three electrode system					Two electrode devices.
	CNF (Fg^{-1})	NCM-LDH (Fg^{-1})	NCM@CNF (1:2) (Fg^{-1})	NCM@CNF (1:1) (Fg^{-1})	NCM@CNF (2:1) (Fg^{-1})	NCM@CNF (2:1) //Activated Carbon asymmetric device (Fg^{-1})
1	27	548	833	1447	1783	348
2	20	468	786	1325	1653	287
3	14	408	755	1265	1595	266
4	10	357	730	1223	1546	253
5	6	308	706	1188	1497	244

Post-cycling morphological evaluation of the NiCoMn-LDH@CNF electrode after 10,000 cycles

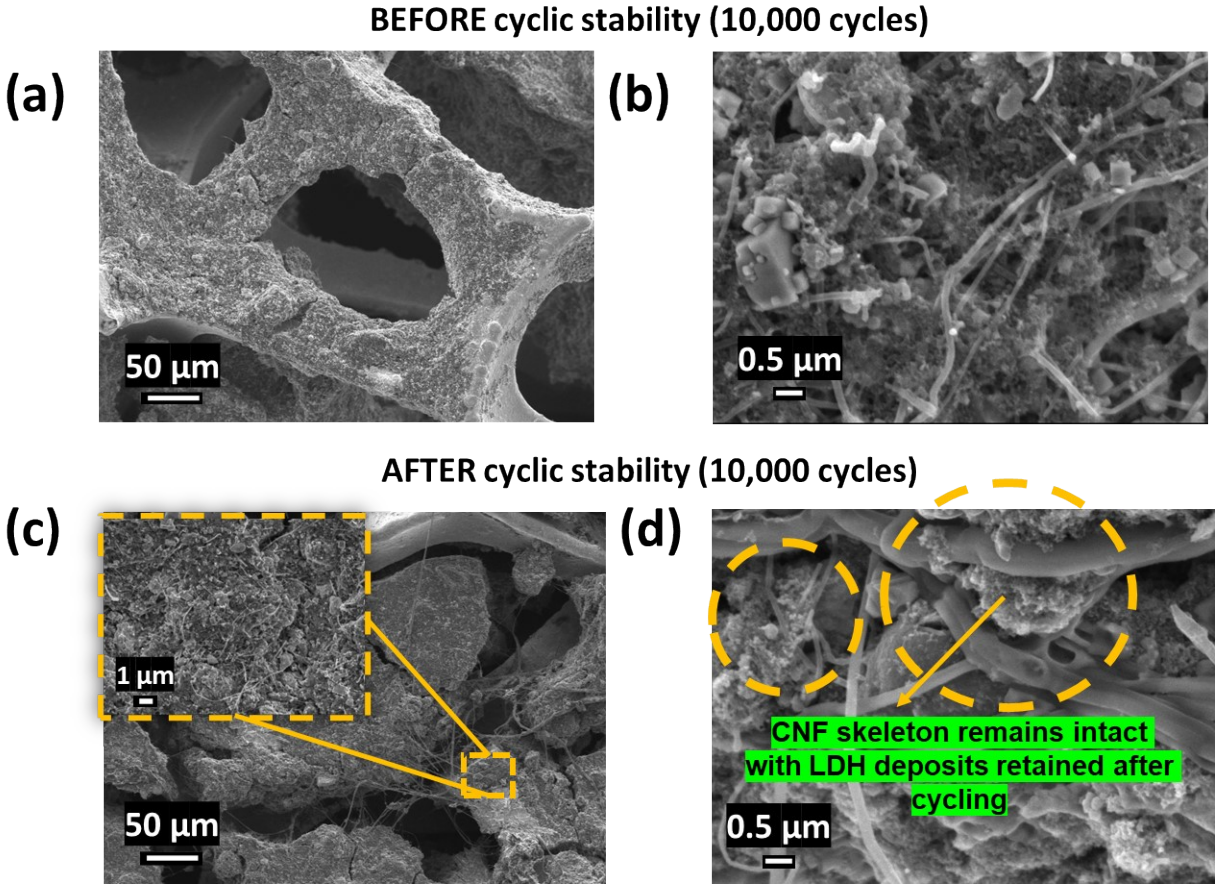

Fig. S5. SEM images of the NiCoMn-LDH@CNF electrode before and after 10,000 charge-discharge cycles: (a) pristine electrode at low magnification showing the macroporous framework, (b) pristine electrode at high magnification displaying LDH distributed over the CNF network, (c) cycled electrode at low magnification revealing preserved structure with slight surface compaction, and (d) cycled electrode at high magnification showing an intact CNF skeleton with retained LDH deposits.

The morphological stability of the NiCoMn-LDH@CNF electrode before and after 10,000 electrochemical cycles was examined using SEM, as shown in Fig. S5(a-d). The pristine electrode (Fig S5a) exhibits a highly porous macroporous structure derived from the nickel foam substrate, providing interconnected pathways for electrolyte diffusion and active material

accommodation. At higher magnification (Fig S5b), the LDH phase is observed to be uniformly distributed and anchored along the CNF network, forming a rough and porous surface favourable for electrochemical activity.

After prolonged cycling, the overall macroporous framework remains intact (Fig S5c), indicating good mechanical stability of the electrode architecture. However, the surface appears relatively denser with the presence of larger aggregated domains, suggesting gradual morphological reorganization of the active material during repeated redox reactions. At higher magnification (Fig S5d), the CNF skeleton is still clearly visible and continuous, with LDH deposits retained along the fiber surfaces. This observation confirms strong interfacial adhesion between LDH and CNF and indicates that the conductive network remains structurally preserved even after extended electrochemical operation.

The slight densification and localized aggregation observed in the cycled electrode may contribute to partial pore narrowing and reduced accessibility of electroactive sites, which can explain the moderate decrease in capacitance retention over long-term cycling. Nevertheless, the absence of severe structural collapse, CNF fracture, or large-scale material detachment demonstrates the robustness of the composite architecture and supports its sustained electrochemical performance after 10,000 cycles.

Post-cycling structural analysis and phase evolution

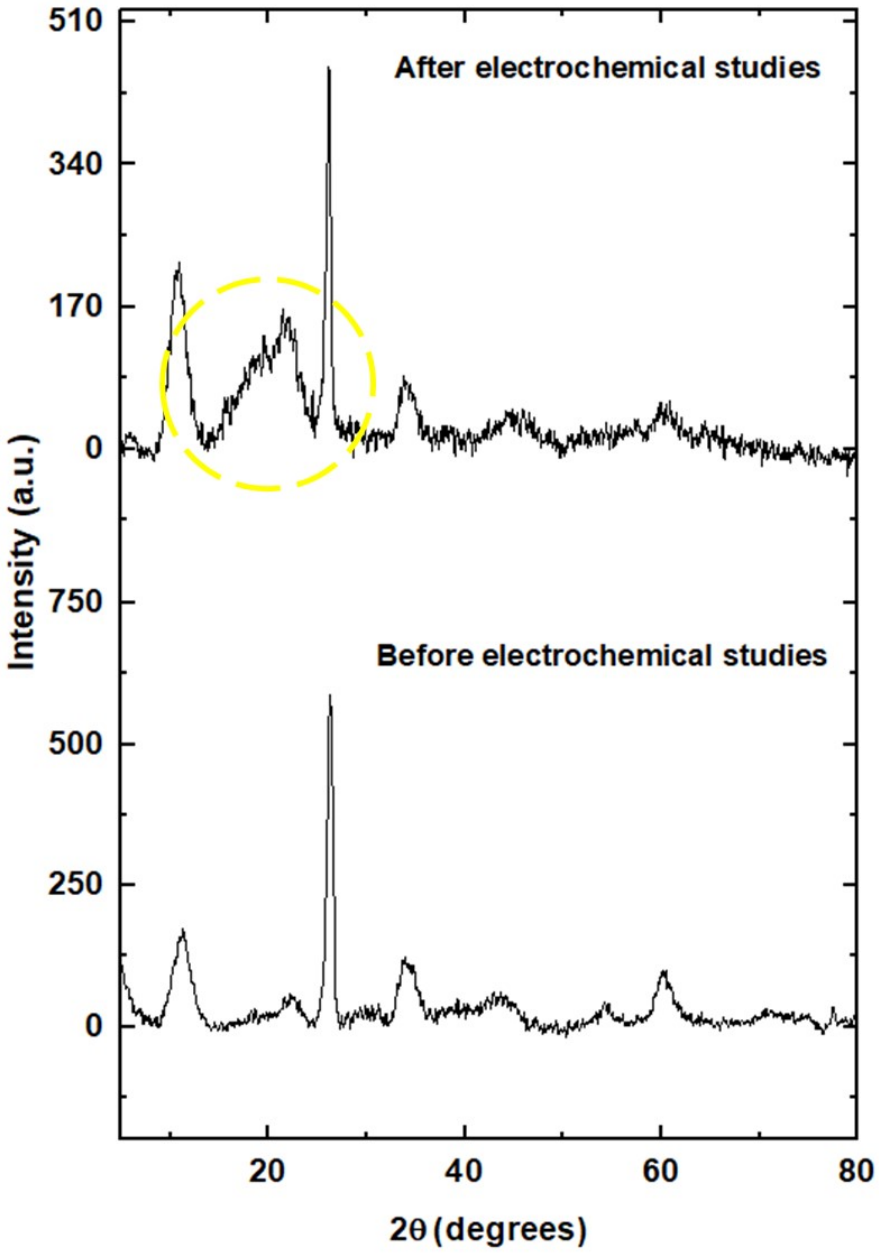

Fig. S6. XRD patterns of NiCoMn-LDH@CNF (2:1) electrode before and after 10,000 electrochemical cycles. The post-cycling pattern shows reduced peak intensity and noticeable peak broadening, particularly in the low-angle region, indicating partial loss of crystallinity, increased microstrain, and structural disorder. No distinct new crystalline impurity phases are observed, suggesting that the material undergoes partial amorphization and structural evolution rather than complete phase transformation during prolonged cycling.

The X-ray diffraction (XRD) patterns of the NiCoMn-LDH@CNF (2:1) electrode before and after 10,000 electrochemical cycles are presented in Fig. S6. After prolonged cycling, the diffraction features exhibit a noticeable reduction in peak intensity along with significant peak broadening, particularly in the low-angle region. These changes indicate a partial loss of crystallinity and the development of structural disorder within the material.[1] The observed peak broadening is primarily attributed to microstrain and a reduction in effective crystallite size. Repeated ion intercalation and deintercalation during electrochemical cycling induce continuous volume expansion and contraction within the layered structure, generating internal stresses.[2] These stresses lead to non-uniform lattice strain, stacking faults, and possible microcracking, all of which contribute to peak broadening. The decrease in diffraction intensity reflects a loss of long-range periodic atomic ordering, suggesting partial amorphization of the LDH phase. In layered materials such as LDHs, low-angle reflections are particularly sensitive to interlayer spacing. The pronounced broadening and distortion in this region indicate that repeated ion insertion/extraction alters the interlayer spacing, disrupts layer stacking, and introduces structural instability.[3] Furthermore, prolonged cycling may induce partial structural reconstruction, including the formation of disordered or nanocrystalline domains and possible surface oxyhydroxide species. These transformations reduce coherent diffraction and contribute to the overall amorphous character observed in the post-cycling pattern. Importantly, despite these changes, no distinct new crystalline impurity phases are observed, suggesting that complete phase transformation does not occur.[4] Instead, the material undergoes partial amorphization and structural evolution while retaining some residual structural features.

Overall, the results indicate that prolonged electrochemical cycling leads to partial structural degradation characterized by increased disorder, microstrain, and amorphization, rather than complete structural collapse. This structural evolution is consistent with the

observed electrochemical behaviour and moderate capacitance retention (~80% after 10,000 cycles).

Interfacial Interaction and Synergistic Effect in NiCoMn-LDH@CNF

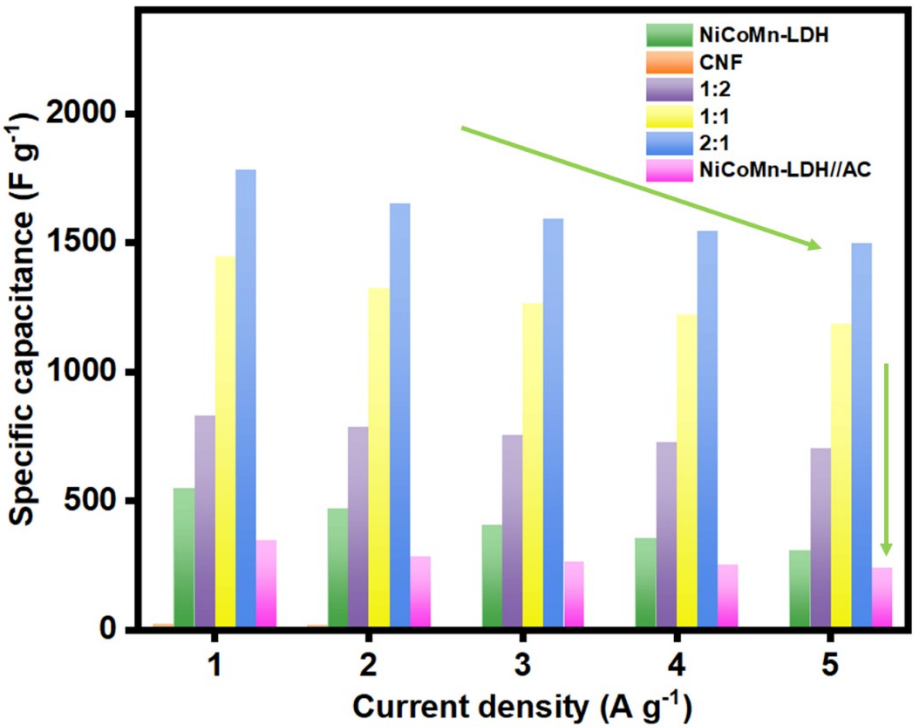

Fig. S7. Specific capacitance of NiCoMn-LDH, CNF, and NiCoMn-LDH@CNF composites with different mass ratios (1:2, 1:1, and 2:1) as a function of current density. The NiCoMn-LDH@CNF (2:1) electrode exhibits superior capacitance and good retention, demonstrating the synergistic effect between LDH and CNF.

The interaction between NiCoMn-LDH and CNFs in the composite is governed by a combination of interfacial and physicochemical effects rather than simple physical mixing. During the ultrasonication-assisted assembly, the LDH nanosheets are uniformly distributed over the CNF network, enabling intimate interfacial contact between the two components.

The CNFs provide a highly conductive and mechanically robust framework, while the NiCoMn-LDH contributes abundant redox-active sites. The interaction between the two phases

is facilitated by surface functional groups present on CNFs (e.g., oxygen-containing groups such as -OH and -COOH), which promote electrostatic interaction and interfacial adhesion with the LDH nanosheets. This results in effective anchoring of LDH onto the CNF surface and prevents agglomeration of active material.

The synergistic effect between NiCoMn-LDH and CNFs is clearly reflected in the electrochemical performance (Fig. S7). The optimized NiCoMn-LDH@CNF (2:1) electrode exhibits significantly higher specific capacitance compared to pristine LDH and CNF, along with improved rate capability. For instance, the composite retains high capacitance (~1497 F g^{-1} at 5 A g^{-1}) compared to ~1783 F g^{-1} at 1 A g^{-1}, demonstrating good capacitance retention with increasing current density.

This enhanced performance arises from the complementary roles of each component: the LDH provides faradaic charge storage through reversible redox reactions, while the CNF network ensures efficient electron transport and structural stability. Although a gradual decrease in capacitance is observed at higher current densities, this behaviour is intrinsic to diffusion-controlled LDH systems and does not indicate the absence of synergy.

Overall, the improved electrochemical performance, together with the structural integration of LDH and CNF, confirms the presence of a synergistic interaction in the composite system.